JOURNAL OF MATERIALS SCIENCE **33** (1998) 497–505

Effect of rare-earth elements on the microstructural characterization in rapidly quenched thermally strengthened aluminium alloys

J. Q. WANG*, B. J. ZHANG, M. K. TSENG
Department of Materials Science, College of Science, P. O. Box 104, Northeastern University, Shenyang 110006, People's Republic of China
G. G. DONCEL
Centro Nacional de Investigaciones Metalurgica, Av. de Gregorio del Amo8, 28040 Madrid, Spain

The influence of rare-earth elements on the microstructural features of rapidly solidified $Al_{93.3-x}Fe_{4.3}V_{0.7}Si_{1.7}Mm_x (x = 0, 0.5, 1.0, 3.0, 6.0)$ alloy was systematically studied by differential scanning calorimetry, X-ray diffraction, transmission electron microscopy and energy dispersive X-ray analysis. Experimental results show that there are different type of phase transformation depending on mischmetal (Mm) concentration. For $Al_{87.3}Fe_{4.3}V_{0.7}Si_{1.7}Mm_{6.0}$ metallic glass, a shoulder was observed on the high-angle side of the main peak in the X-ray diffraction patterns due to quenched-in aluminium nuclei and a prepeak resulting from Mm–Mm pairs. By means of particle extraction analysis, it has been proved that the α-$Al_{13}(Fe, V)_3Si$ phase existing in as-cast Al–Fe–V–Si alloy is wholly or partly inhibited for $Al_{93.3-x}Fe_{4.3}V_{0.7}Si_{1.7}Mm_x$ $(x = 0.5, 1.0, 3.0)$ crystalline alloys. In addition, a new phenomenon has been reported that the lattice parameter of as-quenched Al–Fe–V–Si–Mm alloys decrease with increasing Mm content; the "cell lessening effect". This effect is presumably due to the results of composite interactions between rare-earth elements and alloy elements.

1. Introduction

Techniques of rapid solidification processing (RSP) offer the potential of exploiting unconventional alloy systems owing to the high solid supersaturations (or hypersaturations) of a wide range of alloying elements that may be achieved by cooling at extreme rates from the liquid state. In this regard, much attention has been paid to aluminium-based alloy systems in which efforts have been directed at the development of alloys having a combination of good thermal stability and high strength at temperatures as high as 300–400 °C.

Most of these works have concentrated on the Al–Fe alloy system in which it has been demonstrated that high supersaturations and strength levels can be obtained by quenching ribbons or foils (splats) at rates 10^5–10^6 K s^{-1}. The typical microstructural features of the Al–Fe alloy system have been studied, following the initial work of Jones [1] and later reported by others [2–4], normally contain at least two optically distinct zones. One gives rise to featureless contrast in optical micrographs taken from polished and etched sections, the other exhibiting a marked response. These microstructures were designated Zones A and B, respectively. It was further shown by Thursfield and Stowell [5] that controlled nucleation and growth of metastable second phases (for example, Al_6Fe) [6] during extrusion of splat-cooled Al–Fe alloys lead to relatively high strength and stiffness, because of the obstacles provided to dislocation motion by dispersoids, and to the retention of moderate levels of strength by a high temperature of about 320 °C.

Because all the binary Al–TM alloys are moderately soft and/or they possess only moderate thermal stability, which includes other binary Al–Mn, Al–Cr and Al–Zr alloys, continuing development of optimized high-temperature alloys has focused on ternary and quaternary alloys, with the most prominent of these being Al–Fe alloys, containing additions of cerium [7], molybdenum [8] or vanadium and silicon [9], which promote the formation and retention of favourable metastable phases. The predominent strengthening phases in the alloy Al–8Fe–2Mo is θ-Al_3Fe [8]. In the Al–8Fe–4Ce alloy, the metastable intermetallic phases have been identified as Al_6Fe, $Al_{10}Fe_2Ce$, $Al_{20}Fe_5Ce$ [10]. The intermetallics are generally 100–300 nm in size and provide the dislocation

---

*Author to whom all correspondence should be addressed.

0022–2461 © *1998 Chapman & Hall*

obstacles necessary for strengthening. However, upon annealing for 24 h at 427 °C these metastable phases decompose to equilibrium phases, indicating their limited stability at high temperature.

Alloys in the Al–Fe–V–Si system have been extensively investigated through melt spinning with its optimum cooling rates. The microstructures of the as-cast ribbons can be characterized as either microcellular or discrete silicide dispersoids. The structures are shown to be supersaturated with Fe, V and Si and the intercellular regions to be of b c c α-Al_{13}(Fe, $V)_3Si$ silicide phase, typically ranging in the 50–100 nm diameter size. The good elevated temperature mechanical properties of Al–Fe–V–Si alloys are attributed to the high volume fractions (24–37%) of nanoscale α-Al_{13}(Fe, $V)_2Si$ dispersoids, which have very low coarsening rates ($\sim 10^{-27}$ $m^3 h^{-1}$) compared to other metastable or equilibrium phase in Al–Fe–X alloys [11].

Owing to the influence of elemental cerium (which has a very low solute diffusion in the α-Al matrix) on reducing embrittlement, promoting stability and the degree of supercooling ability in RS Al–Fe alloys, the purpose of the present work was to examine the effect of mischmetal (Mm) elements on the microstructure and thermal stability of dispersion-strengthened Al–Fe–V–Si alloy in order to develop a new class of excellent high-temperature application aluminium alloys.

2. Experimental procedure

2.1. Sample preparation

Alloy ingots of $Al_{93.3-x}Fe_{4.3}V_{0.7}Si_{1.7}Mm_x$($x = 0$, 0.5, 1.0, 3.0, 6.0; at%) were obtained by induction-melting nominal amounts of highly purified elements in an argon atmosphere. The Mm is composed of 55 mass % Ce, 29 mass% La, 11 mass% Nd and 5 mass% Pr. The alloy ingots were then induction melted in a quartz crucible to a superheat of $\sim$100 °C and ejected through a rectangular orifice, by applying argon gas pressure on to a cold copper wheel with a surface velocity of 30 $m s^{-1}$. The resultant ribbons were 20×0.05 mm^2 in average cross-sectional dimensions.

2.2. Sample characterization

Samples cut from continuous ribbons were isochronally annealed in vacuum for 1 h at various temperatures ranging from 100–700 °C. Both non-isothermal and isothermal differential scanning calorimetry (DSC) experiments were carried out in calibrated Perkin–Elmer DSC-7 system under a purified argon atmosphere. In non-isothermal mode, the samples were heated in the temperature range of 27–600 °C with different heating rates of 10, 20, 40 and 80 K min^{-1}. Isothermal experiments were performed at temperatures of 10–40 K below the phase transformation temperature.

The microstructural nature of the as-cast and heated-treated ribbons was verified using X-ray diffraction (XRD), and transmission electron microscopy (TEM) equipped with an energy dispersive X-ray spectrometer (EDX).

2.3. Particle extraction analysis

The average second-phase particle size from the as-quenched samples was less than 50 nm for RS Al–Fe–V–Si–Mm alloys. In order to extract quantitative analysis from these small particles, they had to be removed from the surrounding aluminium matrix. This was achieved using an extraction technique as follows: the polished ribbon specimens were first dissolved in 250 ml methanol containing 10 g iodine and 25 g tartaric acid. Tartaric acid was used to prevent hydrolysis of aluminium ions during the dissolution. When tartaric acid was not used, a gelatinous precipitate of aluminium hydroxide formed. Iodine was chosen as the oxidizing agent instead of bromine. Because reaction rates and temperature rise during dissolution were lower and insufficiently active to etch the surface of this material uniformly in a reasonable time period, the sample was etched for 300 s at 40 °C and rinsed twice in methanol. Then carbon was evaporated on to the surface and the matrix ribbons were dissolved in the former methanol solution. The extraction carbon replicas containing second phase were cut into 3 mm sections and placed on a 3 mm coppergrid. Particle analysis was then performed under a Philips-420 TEM.

2.4. Lattice parameter measurement

The lattice parameter measurement of as-received and heat-treated RS Al–Fe–V–Si–Mm alloys was performed using monochromatic Cu$K\alpha$ radiation over a 2θ range of 10°–85° at a power of 5 kW in a D/max–rB XRD system. The diffractometer was calibrated using a high purity silicon standard for accurate calculation of matrix parameters. The precision of 2θ was about 0.001°. High-order reflections were used in the lattice parameter calculations which were plotted by means of a combination of $\cos^2\theta$ function and the least square method. The extrapolated plot gives the corrected matrix lattice parameter.

3. Results

3.1. Thermal analysis

Fig. 1a–e are the DSC traces for glassy and crystalline $Al_{93.3-x}Fe_{4.3}V_{0.7}Si_{1.7}Mm_x$ ($x = 0$, 0.5, 1.0, 3.0, 6.0) alloys. It is apparent that the phase transformation in these five alloys goes through different processes. In amorphous $Al_{87.3}Fe_{4.3}V_{0.7}Si_{1.7}Mm_{6.0}$ alloy, three exothermic peaks, corresponding to different crystallization temperatures, are present. At a heating rate of 20 °C min^{-1} three onset and peak temperatures (T_s, T_p) of phase transformation are (483, 500 K), (624, 630 K) and (720, 733 K), respectively. This fact indicates that more than one crystallization process occurs until all the material becomes crystalline. For $Al_{93.3-x}Fe_{4.3}V_{0.7}Si_{1.7}Mm_x$ ($x = 0.5$, 1.0, 3.0), three crystalline alloys, there are two phase transformations at $T_p = 641$ and 708 K for 3.0 at% Mm

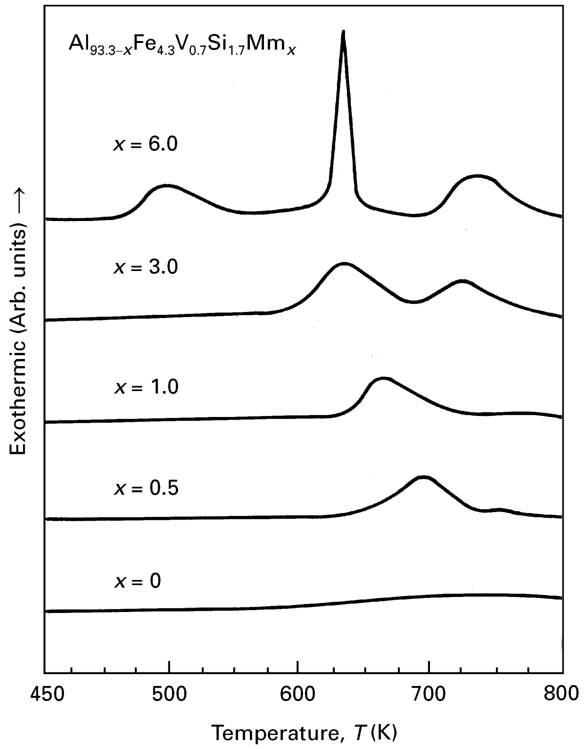

Figure 1 DSC scans obtained from as-quenched rapidly solidified Al–Fe–V–Si–Mm alloys at a heating rate of 20 °C min^{-1}.

alloy, one phase transformation at $T_p = 673$ K and 683 K for 0.5 at % and 1.0 at % Mm alloys, respectively. However, for $Al_{87.3}Fe_{4.3}V_{0.7}Si_{1.7}$ alloy, no phase transformation was detected.

The dependence of the crystallization temperatures on heating rate can be determined with the associated activation energies, Q, by means of Kissinger's peak shift method [12]. The plots in Fig. 2 are all the activation energies for $Al_{87.3}Fe_{4.3}V_{0.7}Si_{1.7}Mm_{6.0}$ glassy alloy. The values for the second peak ($Q = 261$ kJ mol^{-1}) and the third peak ($Q = 222$ kJ mol^{-1}) are lower than that for devitrification ($Q = 332$ kJ mol^{-1}), indicating a comparatively high glass stability.

Isothermal crystallization studies can reveal the nature of the glass to crystal reaction and provide powerful additional information on the kinetics analysis of the phase transformation. The isothermal results from $Al_{87.3}Fe_{4.3}V_{0.7}Si_{1.7}Mm_{6.0}$ amorphous alloy are shown in Fig. 3 which reveals a maximum value of the exothermic reaction at $t_a = 0$, and no incubation stage is seen. The absence of the incubation stage is independent of annealing temperature. The abnormal isothermal DSC phenomenon without an incubation stage is due to the pre-existence of crystalline nuclei in the as-cast amorphous structure, which is consistent with a low crystalline onset temperature, T_x, and no detectable glass transition temperature, T_g,

3.2. As-melt-spun microstructure

Typical microstructures of $Al_{93.3-x}Fe_{4.3}V_{0.7}Si_{1.7}Mm_x$ ($x = 0, 0.5, 1.0, 3.0, 6.0$) alloys in the rapidly solidified condition are shown in Fig. 4a–d. It can be seen that the microstructures of these penternary alloys exhibit a refined microcellular structure, based

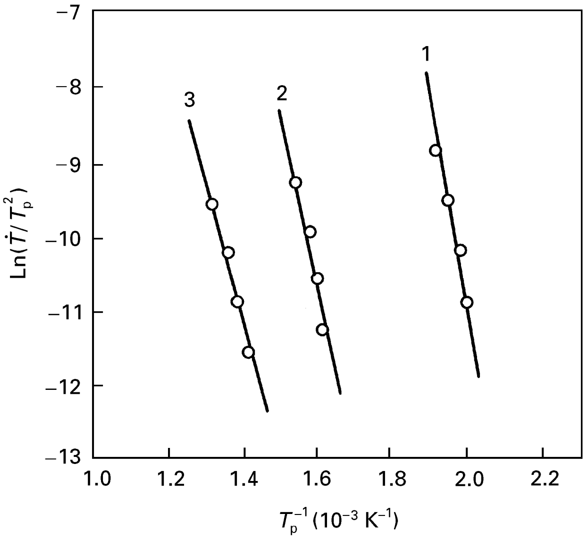

Figure 2 Kissinger plots for calculating the activation energy of Al–Fe–V–Si–Mm metallic glass 1, first peak; 2, second peak; 3, third peak

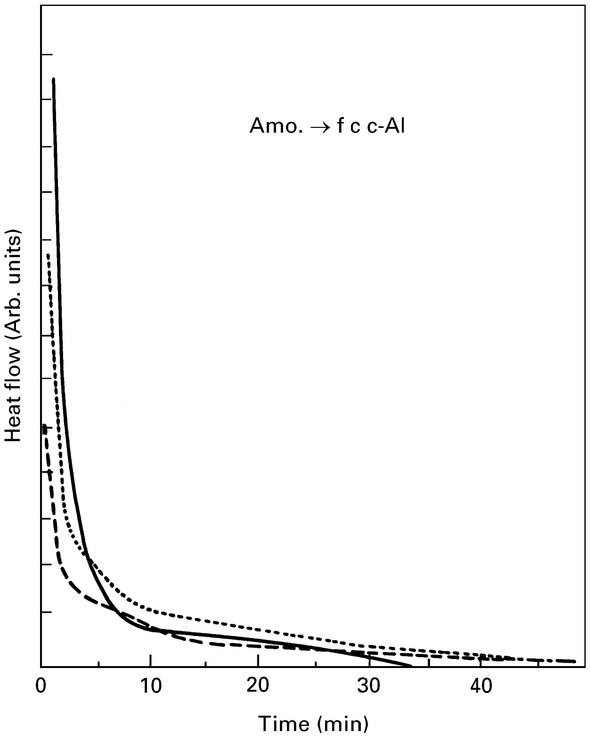

Figure 3 Isothermal DSC thermograms of Al–Fe–V–Si–Mm amorphous alloys annealed at 453, 463 and 473 K.

on α-Al, with second phases present in the intercellular regions, except for $Al_{87.3}Fe_{4.3}V_{0.7}Si_{1.7}Mm_{6.0}$ amorphous alloy. In the meantime, there is a tendency for the particle size, d, and the interparticle spacing, λ, to decrease with increasing Mm content. In order to examine the effect of Mm elements on the formation of fine second phase, the X-ray diffraction patterns of the as-cast Al–Fe–V–Si–Mm alloys were taken and the results are shown in Fig. 5. As previously reported [11], the microstructure in the RS Al–Fe–V–Si alloy consists of mixed aluminium and α-$Al_{13}(Fe, V)_3Si$ phases. For $Al_{87.3}Fe_{4.3}V_{0.7}Si_{1.7}Mm_{6.0}$ metallic glass, it can be noticed that a distinct additional shoulder

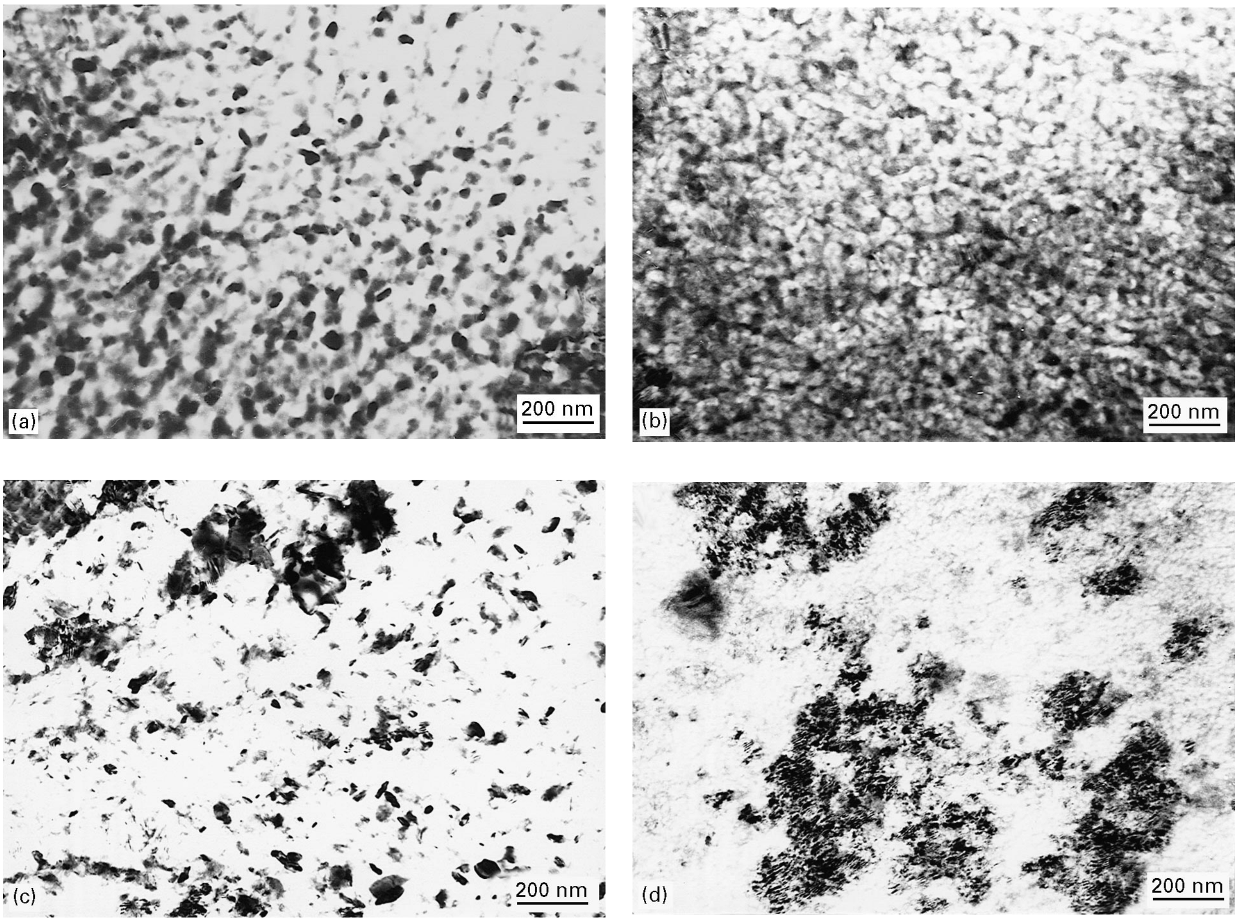

Figure 4 Transmission electron micrographs of as-melt-spun $Al_{93.3-x}Fe_{4.3}V_{0.7}Si_{1.7}Mm_x$ penternary alloys: (a) $x = 0$, (b) $x = 0.5$, (c) $x = 1.0$, (d) $x = 3.0$. (○) Al, (▲), α-Al_{13} (Fe, V)$_3$ Si.

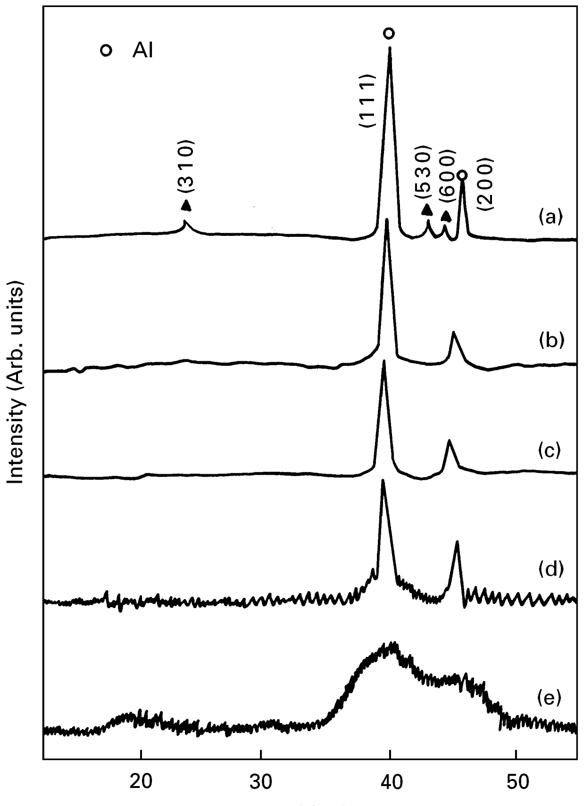

Figure 5 X-ray diffraction patterns of as-quenched $Al_{93.3-x}Fe_{4.3}V_{0.7}Si_{1.7}Mm_x$ alloys: (a) $x = 0$, (b) $x = 0.5$, (c) $x = 1.0$, (d) $x = 3.0$ (e) $x = 6.0$.

structure near $2\theta = 38°$ and a prepeak at $2\theta = 18.5°$ appear, suggested to correspond to Al–Fe series and Ce(La)–Ce(La) short-range ordering [13], respectively. However, no diffraction peaks for second phases in the three $Al_{93.3-x}Fe_{4.3}V_{0.7}Si_{1.7}Mm_x$ ($x = 0.5, 1.0, 3.0$) crystalline alloys are detected, because their size is not greater than 50 nm.

With the aim of examining the second phases shown in Fig. 4b–d in the Mm concentration range from 0.5–3.0 at %, particle extractions were made as described, and subsequently the microstructural type and composition of these second phases were indicated using XRD, selected-area electron diffraction (SAED) and EDX method. The observed *d* spacings and relative intensities of the dispersive particles existing in $Al_{92.8}Fe_{4.3}V_{0.7}Si_{1.7}Mm_{0.5}$ and $Al_{93.3}Fe_{4.3}V_{0.7}Si_{1.7}Mm_{1.0}$ alloys are shown in Table I. The table indicates that there are mixed α-$Al_{13}(Fe, V)_3Si$ and metastable Al_8Fe_4Mm phases for the 0.5 at% Mm alloy and a single Al_8Fe_4Mm second phase for the 1.0 at % Mm alloy. Because the particle size is less than 10 nm in the $Al_{90.3}Fe_{4.3}V_{0.7}Si_{1.7}Mm_{3.0}$ alloy, it is very difficult accurately to determine the microstructural type of particles through their weak XRD intensities and extremely dispersive diffraction rings of SAED. However, in our previous work [14], we found that the Mössbauer spectrum (ME) of $Al_{90.3}Fe_{4.3}V_{0.7}Si_{1.7}Mm_{3.0}$ crystalline alloy exhibits two broad lines

TABLE I X-ray diffraction data from the extracted second phase in as-quenched Al–Fe–V–Si–Mm alloys

$Al_{93.3-x}Fe_{4.3}V_{0.7}Si_{1.7}Mm_x$ (at%)			
$x = 1.0$		$x = 0.5$	
d(nm)	I/I_{max}	d(nm)	I/I_{max}
0.637[a]	14	0.437[a]	37
0.439[a]	38	0.397[b]	19
0.366[a]	11	0.366[a]	13
0.318[a]	20	0.277[a]	48
0.276[a]	50	0.255[a]	40
0.257[a]	43	0.247[b]	15
0.252[a]	20	0.221[a]	51
0.220[a]	57	0.216[b]	59
0.208[a]	100	0.210[b]	27
0.198[a]	40	0.208[a]	78
0.187[a]	21	0.204[b]	100
0.181[a]	10	0.196[a]	37
		0.186[a]	20
		0.127[b]	19

[a] Al_8Fe_4Mm, $a = 0.886$ nm, $b = 0.508$ nm, tetragonal
[b] α-$Al_{13}(Fe, V)_3Si$: $a = 1.260$ nm, b c c.

resulting from the distribution, $P(\Delta)$, of the quadrupole splitting, (Δ), and characteristic of the ME spectra of amorphous and quasicrystalline alloys or the quasicrystalline second phase contained in the crystalline alloy. Thus, it may be inferred that the superfine second phase in $Al_{90.3}Fe_{4.3}V_{0.7}Si_{1.7}Mm_{3.0}$ alloy belongs to the quasicrystalline phase. In addition, the results of EDX show that the composition of this phase is about $Al_{20}Fe_5Mm$, in good agreement with that of the quasicrystalline phase reported by Ayer *et al.* [10].

In the as-solidified condition, the aluminium lattice constant values of these penternary alloys were measured, as shown in Table II. It was found that there is a tendency for lattice parameter to decrease with increasing Mm concentration. We call this abnormal phenomenon "cell lessening effect". The reason for this phenomenon will be discussed in Section 4.

3.3. Effect of heat treatment

According to the DSC results (see Fig. 1), apparently there are different types of phase transformation for Al–Fe–V–Si–Mm penternary alloys. It has been determined that the three-step crystallization of amorphous $Al_{87.3}Fe_{4.3}V_{0.7}Si_{1.7}Mm_{6.0}$ alloy can be represented as follows [15]

$$\begin{aligned} &AM \rightarrow AM' + \alpha\text{-Al} \\ &\rightarrow \alpha\text{-Al} + Al_{11}Mm_3 + i\text{-phase} \\ &\rightarrow \alpha\text{-Al} + Al_{11}Mm_3 + i\text{-phase} + i'\text{-phase}, \qquad (1) \end{aligned}$$

where the stoichiometic i-phase about $Al_{32}(Fe, V)Si_{12}$, i'-phase is a compound of two kinds of particle, their chemistries are $Al_{24}(Fe, V)S_{18}$ and $Al_{40}(Fe, V)Si_2$, respectively. In addition, we have proved that the latter two-step phase transformation is present exactly in $Al_{90.3}Fe_{4.3}V_{0.7}Si_{1.7}Mm_{3.0}$ alloy, except for the first precipitation of α-Al phase. For $Al_{93.3-x}Fe_{4.3}V_{0.7}Si_{1.7}Mm_x$ ($x = 0.5$, 1.0) crystalline alloys, only a one-step phase transformation exists, which results from the disappearance of metastable Al_8Fe_4Mm phase and the reappearance of α-$Al_{13}(Fe, V)_3Si$ phase during the heat-treatment process. The reason for the absence of metastable Al_8Fe_4Mm phase isostructural to Al_8Fe_4Ce [16] might be due to the continuous precipitation of elemental vanadium and silicide after high-temperature ageing treatment, which originally exist in the α-A matrix in the solid-solution state in as-cast alloys. Table III lists the d-spacings and relative intensities for these penternary alloys after heat treatment at 400 °C for 1 h. The corresponding micromorphologies were obtained simultaneously as shown in Fig. 6. It is noticeable that there is a better homogeneous particle dispersive state and finer particle size in $Al_{93.3-x}Fe_{4.3}V_{0.7}Si_{1.7}Mm_x$ ($x = 0.5$, 1.0) alloys than is present in $Al_{93.3}Fe_{4.3}V_{0.7}Si_{1.7}$ alloy in the high-temperature state. This indicates a new direction for future development of high-temperature alloys of this type by means of the good interaction of alloying additions that have low solubility diffusivities in aluminium.

4. Discussion

For rapidly solidified $Al_{87.3}Fe_{4.3}V_{0.7}Si_{1.7}$ (at%) alloy, as shown in Fig. 4(a), an unusual microstructural feature is the presence of dispersive α-$Al_{13}(Fe, V)_3Si$ particles having a very low coarsening rate. The reason for the formation of these randomly oriented intermetallic compounds could be explained more reasonably by the dispersoids being considered to form prior to the aluminium cell, i.e. as a primary phase, although there are other theories that suggest they form by "microeutectic" solidification [17], solid-state precipitation [18] or crystallization of an intercellular amorphous phase [19, 20]. A reasonable explanation is that a high nucleation rate of these α-$Al_{13}(Fe, V)_3Si$ intermetallic particles, combined with a low growth rate (and little growth time), could result in a very fine dispersion of particles in the

TABLE II The matrix lattice parameter values of as-cast Al–Fe–V–Si–Mm alloys

	$Al_{93.3-x}Fe_{4.3}V_{0.7}Si_{1.7}Mm_x$				
	$x = 0$	$x = 0.5$	$x = 1.0$	$x = 3.0$	$x = 6.0$
α-Al (nm)	0.404 346	0.404 010	0.403 641	0.403 554	0.403 171[a]

[a] This value is regarded as a reference

TABLE III X-ray diffraction data showing *d*-spacings and relative intensities for Al–Fe–V–Si–Mm alloys

$Al_{93.3-x}Fe_{4.3}V_{0.7}Si_{1.7}Mm_x$ (at%) alloy, aged 400 °C/1 h							
$x = 0.5$		$x = 1.0$		$x = 3.0$		$x = 6.0$	
d(nm)	I/I_{max}	d(nm)	I/I_{max}	d(nm)	I/I_{max}	d(nm)	I/I_{max}
0.398[a]	26	0.407[a]	9	0.616[b]	8	0.406[c]	19
0.362[a]	10	0.397[a]	21	0.406[c]	14	0.402[c]	18
0.304[a]	6	0.363[a]	9	0.402[c]	16	0.312[c]	14
0.278[a]	7	0.336[a]	20	0.312[c]	13	0.280[b]	31
0.246[a]	10	0.319[a]	4	0.280[b]	28	0.269[c]	22
0.242[a]	4	0.282[a]	10	0.269[c]	23	0.268[c]	21
M 0.235[d]	> 100	0.277[a]	7	0.268[a]	19	0.265[c]	43
0.215[a]	42	0.246[a]	8	0.265[c]	41	0.244[b]	31
0.212[a]	5	0.240[a]	6	0.244[b]	29	M0.235	100
0.210[a]	19	M 0.234	> 100	M 0.235	100	M 0.202	51
0.204[a]	59	0.216[a]	44	M 0.202	48	0.171[c]	11
M 0.202	100	0.212[a]	6	0.198[b]	12	0·.170[c]	11
0.199[a]	11	0.210[a]	21	0.189[b]	15	M 0.142	19
0.189[a]	7	0.204[a]	63	0.171[c]	10		
0.160[a]	4	M 0.202	100	0.170[c]	9		
M 0.143	27	0.199[a]	10	M 0.142	21		
0.127[a]	12	0.187[a]	6	0.126[b]	9		
0.125[a]	3	0.177[a]	5	M 0.122	19		
M 0.122	25	M 0.143	24				
		0.132[a]	7				
		0.127[a]	10				
		0.126[a]	5				
		M 0.122	21				

[a] α-$Al_{13}(Fe, V)_3$ Si: $a = 1.260$ nm, b c c.

[b] *i*-phase: its stoichiometry is $Al_{32}(Fe, V)Si_{12}$.

[c] $Al_{11}Mm_3$ isostructural to $A_{11}Ce_3$: $a = 0.443$ nm, $b = 1.013$ nm, $c = 1.314$ nm orthorhombic.

[d] M = matrix.

undercooled liquid. The subsequent advice of the aluminium front would cause them to be pushed and trapped in the intercellular regions of the microcell, at higher interfacial velocities, and engulfed by a planar aluminium front in a randomly oriented fashion. Thus, the microstructural features may, indeed, be a result of high-temperature formation of the α-$Al_{13}(Fe, V)_3Si$ dispersoids from the melt.

High cooling rates in rapidly solidified processing can widen the concentration range of lanthanum or cerium rare-earth elements in an aluminium matrix either by increasing miscibility, or by the formation of finely dispersed, rare-earth-rich second phase. Excess lanthanum or cerium, which was not trapped in the matrix during solidification, segregates to the grain boundaries. In our experiments, the distinct characterization is the tendency to form fine regions and the whole or partial disappearance of spherical α-$Al_{13}(Fe, V)_3Si$ dispersive dispersoids while adding mischmetal elements (0.5, 1.0, 3.0 at % content) to Al–Fe–V–Si alloy. The tendency to form finer regions on addition of rare-earth elements could be explained by the possible lowering of the liquidus which reduces the liquidus–solidus temperature ranges ($\Delta T_{LS} = T_L - T_S$). This will reduce the segregation during cooling. The reduction of ΔT_{LS} is possible because of high eutectic composition, C_E, of Al–rare-earth binaries. For example, the C_E for Al–Ce(La) is 12 wt %, while C_E of Al–Fe is only 1.8 wt %. In view of the dispersoids forming as a primary phase, the motive forces of the Al_8Fe_4Mm phase in place of the α-$Al_{13}(Fe, V)_3Si$ phase, mainly come from the strong interaction between aluminium and Mm elements as well as the satisfaction of thermodynamic conditions.

With the increasing concentration of Mm elements in Al–Fe–V–Si base alloy, the tendency of alloy amorphism was enhanced and a new amorphous $Al_{87.3}Fe_{4.3}V_{0.7}Si_{1.7}Mm_{6.0}$ alloy was produced. As is evident from the Al–Ce equilibrium phase diagram shown in Fig. 7, the glass-formation range lies in the compositional range between a eutectic point at 3.0 at % Ce and an $Al_{11}Ce_3$ compound [21]. The melt-quenched phase at the eutectic composition with the lowest melting temperature of 910 K is composed only of the f c c solid solution. A similar relationship between the melt-quenched structure and the equilibrium diagram is also recognized in Al–La, Al–Nd and Al–Pr systems. It is empirically known that the glass formation of binary alloys by liquid quenching necessitates that (1) the atomic size ratio of the constituent atoms below about 0.8, and (2) the interaction between the constituent atoms be attractive and the mixing enthalpy be relatively large. These two factors have been proved by Inoue *et al.*'s [22] systematic study on the glass formation in Al–Ce and Al–La alloys; they also pointed out that the lowest cerium or lanthanum concentration from amorphous Al–Ce(La) alloys is 7.0 at %. Because there is 6.0 at % Mm concentration in our $Al_{87.3}Fe_{4.3}V_{0.7}Si_{1.7}Mm_{6.0}$ amorphous alloy, it

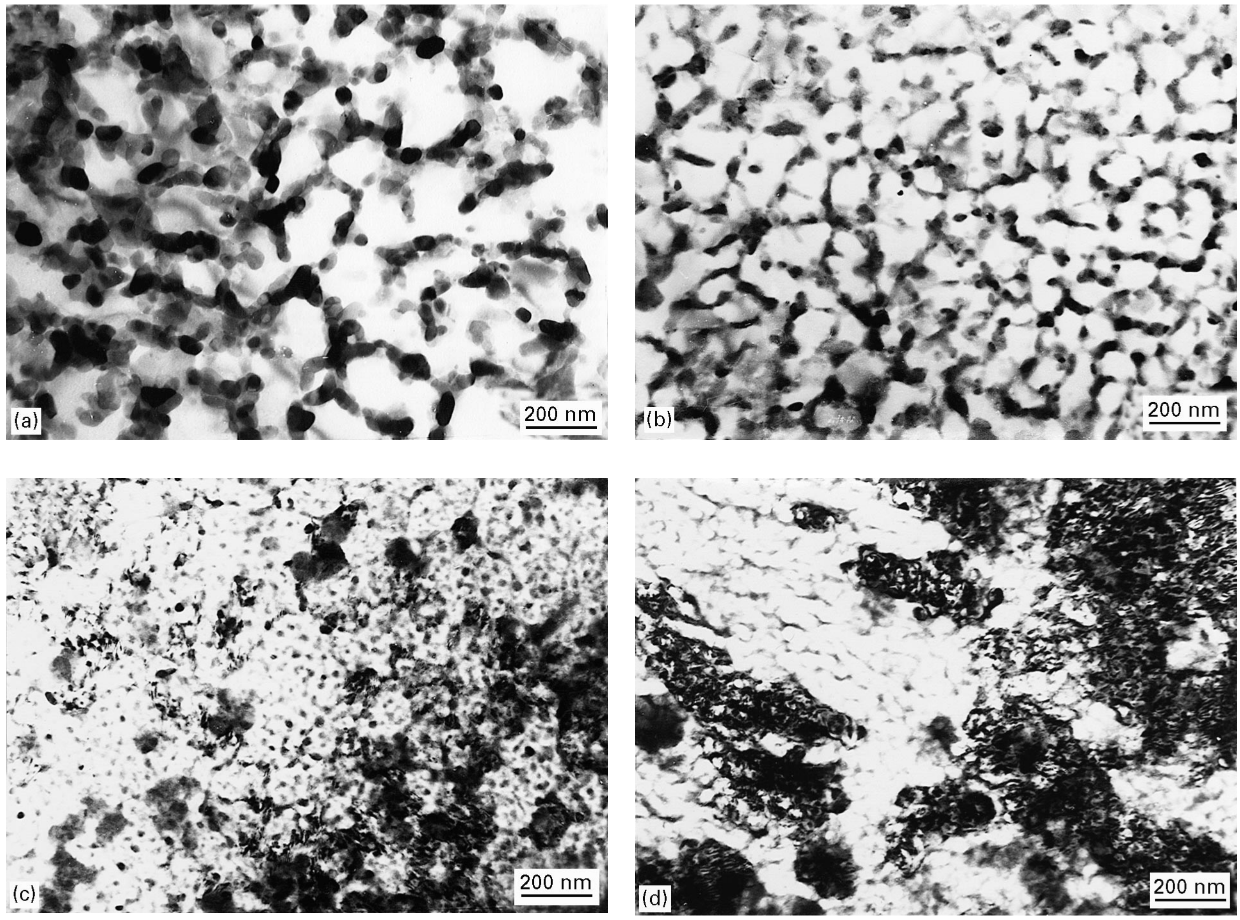

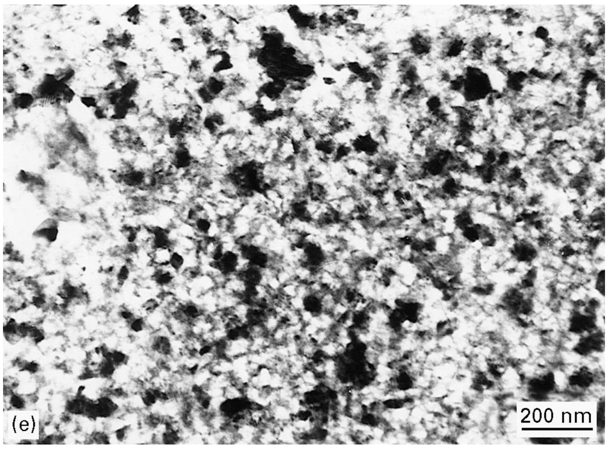

Figure 6 TEM microstructures $Al_{93.3-x}Fe_{4.3}V_{0.7}Si_{1.7}Mm_x$ alloy ribbons after annealing at 400 °C for 1 h (a) $x = 0$, (b) $x = 0.5$, (c) $x = 1.0$, (d) $x = 3.0$ (e) $x = 6.0$.

is reasonable that Mm and M(≡ Fe, V) or aluminium and M may play some role in the formation of Al–Fe–V–Si metallic glass.

Equilibrium phase diagrams of Ce(La)–M binary alloys indicate that the bonding nature of Ce(La) with M can be classified into two groups: elemental iron, cobalt and nickel, with an attractive bonding nature to the formation of intermetallic compounds, and elemental vanadium, niobium and chromium, with a repulsive nature, lead to an immiscibility gap. In addition, the atomic structure of amorphous $Al_{90}Fe_xCe_{1-x}$ has been investigated by neutron and X-ray scattering [23, 24]. It was found that in these amorphous alloys, the distance of an Fe–Al pair of 0.02 nm shorter than the sum of the atomic radii of aluminium and iron suggesting strong interaction between these two elements. The strong Al–Fe interaction suggested from the structural analysis is in agreement with the large negative volume additivity of the Al–Fe alloys in the liquid or solid state [25]. The X-ray profile of amorphous $Al_{87.3}Fe_{4.3}V_{0.7}Si_{1.7}Mm_{6.0}$ alloy (see Fig. 5), proves the existence of the typical near-neighbour distance of the Al–Fe series and the Ce(La)–Ce(La) short-range ordering with an aluminium atomic sandwich plate. Thus, based on the above discussion, the unusual glass formability in Al–Fe–V–Si–Mm penternary alloy could be attributed to the simultaneous existence of the strong interactions of the Al–Ce(La) and Al–Fe as well as the atomic size differential effect between rare-earth and metal elements. For $Al_{93.3-x}Fe_{4.3}V_{0.7}Si_{1.7}Mm_x$ ($x = 5$, 1.0, 3.0 at %) crystalline alloys, the strong attractive bonding nature of Al–La(Ce), Al–Fe and Ce(La)–Fe, and the repulsive bonding nature of Ce(La)–V, result in the appearance of ternary Al_8Fe_4Mm metastable phase, no vanadium nor silicon content, and the suppression of α-$Al_{13}(Fe, V)_3Si$ second phase existing in Al–Fe–V–Si base alloy from the melt.

During the course of exploring the effect of rare-earth elements on crystal structural parameters in RS aluminium-based alloys, it is usual to accept that rare-earth elements cause the increase in the lattice constant of aluminium. However, in the present paper, by using the accurate method of X-ray diffraction at the slower scanning speed, the results showed that the aluminium matrix lattice parameters decrease with

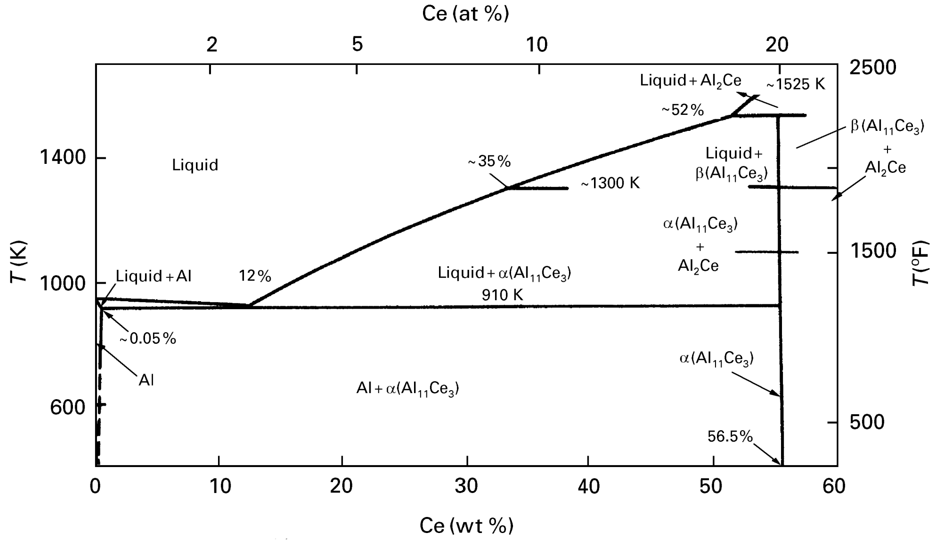

Figure 7 Phase diagram of the Al–Ce binary system

increasing rare-earth element content in as-cast Al–Fe–V–Si–Mm alloys as shown in Table II; similar results were obtained in the study of Al–Mg–Si alloy [26]. This abnormal phenomenon caused by rare-earth elements is called a "cell lessening effect". According to our research results on the changes of iron atomic configurations in as-cast Al–Fe–V–Si–Mm alloys by means of Mössbauer spectroscopy [14], the atomic content of iron in α-Al solid solution tends to decline with the Mm concentration from 0.5 at % to 3 at %. Therefore, the decrease of the matrix lattice parameter may be attributed to the following two situations. One situation is the increase in the solid solution of the vanadium and silicon elements in the matrix, because of the existence of the Al_8Fe_4Mm phase containing neither of the above two elements and the enhancement of the degree of supercooling. It has been reported in the literature that vanadium and silicon elements in aluminium solid solution can effectively diminish the lattice parameter [27]. The other situation is related to the existing states of the rare-earth elements in the matrix. It is well known that there are two kinds of interstitial positions having the sizes of 0.1170 and 0.062 nm, corresponding to octahedral and tetrahedral intervals, respectively. Owing to the strong polarizable action between rare-earth elements and metalloid silicon element, the atomic radii of rare-earth elements could be diminished distinctively. For example, the covalent radius of lanthanum element is 0.1877 nm which becomes 0.1277 nm in the 60% ionic state and finally 0.1061 nm in the 100% ionic state. Thus, at this time, rare-earth elements could dissolve in the matrix in an interstitial way and simultaneously improve the mutual dissolution of alloy elements. Hence, the "cell lessening effect" may be regarded as the result of composite interactions between rare-earth elements and alloy elements.

5. Conclusions

1. A three-stage crystallization sequence is identified in the $Al_{87.3}Fe_{4.3}V_{0.7}Si_{1.7}Mm_{6.0}$ amorphous alloy. The X-ray diffraction patterns show a shoulder on the high-angle side of the main peak, due to quenched-in aluminium nuclei and a prepeak coming from Mm-Mm pairs.

2. By using the particle extraction analysis of as-quenched Al–Fe–V–Si–Mm crystalline alloys, it was found that α-$Al_{13}(Fe, V)_3Si$ and Al_8Fe_4Mm phases coexist for 0.5 at % Mm alloy, with only the appearance of Al_8Fe_4Mm phase for 1.0 at % Mm alloy and quasicrystalline $Al_{20}Fe_5Mm$ phase for 3.0 at %Mm alloy.

3. TEM observations illustrate that there is a tendency for the particle size and the interparticle spacing to decrease with increasing Mm content in the as-cast Al–Fe–V–Si–Mm alloys and the reappearance of α-$Al_{13}(Fe, V)_3Si$ phase after heat treatment above 400 °C for 0.5 and 1.0 at % Mm alloys.

4. The reason for the formation of Al–Fe–V–Si–Mm metallic glass can be attributed to the simultaneous existence of the strong interactions of Al–Ce(La) and Al–Fe, as well as the atomic size differential effect between rare-earth elements and metal elements.

5. The phenomenon of the decreasing lattice parameter of as-cast Al–Fe–V–Si–Mm alloys with increasing Mm content, the "cell lessening effect", is observed by means of accurate XRD measurement. This effect presumably results from composite interactions between rare-earth elements and metal elements.

Acknowledgements

The authors thank Professor Xiu-Fang Chen, Vice-Professor Cun-Fu Qian and Vice-Professor Yue-Sheng Chao, for useful discussions. The financial support of the Chinese National Natural Science Foundation (CNNSF) and State Key Laboratory of RSA, Academic Sinica, is gratefully acknowledged.

References

1. H. JONES, *Mater. Sci. Engng* **5** (1969–1970) 1.
2. S. SRIRAM and J. A. SEKHAR, *J. Mater. Sci. Lett.* **66** (1984) L9.

3. T. H. SANDERS, H. G. PARIS and J. W. MULLINS, in "Rapidly Solidified Amorphous and Crystalline Alloys", edited by B. H. Kear, B. C. Giessen and M. Cohen (Elsevier, New York, 1982) p. 369.
4. L. J. MASUR, J. T. BURKE, T. Z. KATTAMIS and M. C. FLEMINGS, *ibid.* p. 185.
5. G. THURSFIELD and M. T. STOWELL, *J. Mater. Sci.* **9** (1974) 1644.
6. M. H. JACOBS, A. G. DOGGETT and M. J. STOWEL, *Mater. Sci. Engng* **9** (1974) 1631.
7. K. N. RAMAKRISHNAN, H. B. MOSHANE, T. SHEPPARD and E. K. IOANNIDIS, *Mater. Sci. Technol.* **8** (1992) 709.
8. C. M. ADAM, in "Rapidly Solidified Amorphous and Crystalline Alloys", edited by B. H. Kear, B. C. Giessen and M. Cohen (Elsevier, New York, 1982) p. 411.
9. D. J. SKINNER, R. L. BYE, D. RAYBOULD and A. M. BROWN, *Scripta Metall.* **20** (1986) 867.
10. R. AYER, L. M. ANGERS, R. R. MUELLER, J. C. SCALON and C. F. KLEIN, *Metall. Trans.* **19A** (1988) 1645.
11. L. A. DAVIS, S. K. DAS, J. C. M. LI and M. S. ZEDALIS, *Int. J. Rapid Solidif.* **8** (1994) 112.
12. H. E. KISSINGER, *Anal. Chem.* **29** (1957) 1702.
13. J. Q. WANG, B. J. ZHANG and M. K. TSENG, *J. Mater. Sci. Lett.* **14** (1995) 1403.
14. WANG JAIN-QIANG, CAO YUE-SHENG, ZENG MEI-GUANG, ZHANG BAO-JIN and CHEN XIU-FANG, *J. Rare Earths*, **14** (1996) 201.
15. J. Q. WANG, C. F. QIAN, M. K. TSENG and M. Q. LU, *Scripta Metall.* **32** (1995) 663.
16. S. SRIRAM and J. A. SEKHAR, *Mater. Sci. Engng* **66** (1984) L9–L13.
17 M. H. JACOBS, A. G. DOGGETT and M. J. STOWELL, *J. Mater. Sci.* **9** (1974) 1631.
18. R. D. FIELD, J. W. ZINDEL and H. L. FRASER, *Scripta Metall.* **20** (1986) 415.
19. L. A. BENDERSKY, M. J. KAUFMAN, W. J. BOETTINGER and F. S. BIANCANIELLO, *Mater. Sci. Engng* **98** (1988) 213.
20. L. A. BENDERSKY, A. J. MCALISTER and F. S. BIANCANIELLO, *Metall. Trans.* **19A** (1988) 2893.
21. T. B. MASSALSKI, "Binary Alloy Phase Diagram" (American Society for Metals, Metals Park OH, 1986) Vol. 1, p. 100.
22. A. INOUE, K. OHTERA and T. MASUMOTO, *Jpn J. Appl. Phys.* **27** (1988) 736.
23. H. Y. HSIEH, B. H. TOBY, T. EGAMI, Y. HE, S. J. POON and G. J. SHIFLET, *J. Mater. Res.* **5** (1990) 2807.
24. H. Y. HSIEH, T. EGAMI, Y. HE, S. J. POON and G. J. SHIFLET, *J. Non-Cryst. Solids* **135** (1991) 248.
25. D. TURNBULL, *Acta Metall. Mater.* **38** (1990) 243.
26. ZHANG MI-LIN, JING XIAO-YAN, LU HUA-YI and TANG DING-XIANG, *J. Rare Earths* **11** (1992) 74.
27. S. STEEB and H. WARLIMONT (eds), "Proceedings of the Fifth International Conference on Rapidly Quenched Metals", Vol I, (Elsevier Science, Amsterdam, 1985) p. 899.

Received 19 April 1996
and accepted 17 April 1997